J|A|C|S
ARTICLES
Published on Web 08/26/2004

A Homologous Series of Regioselectively Tetradeprotonated Group 8 Metallocenes: New Inverse Crown Ring Compounds Synthesized via a Mixed Sodium−Magnesium Tris(diisopropylamide) Synergic Base

Prokopis C. Andrikopoulos,[†] David R. Armstrong,[†] William Clegg,[‡] Carly J. Gilfillan,[†] Eva Hevia,[†] Alan R. Kennedy,[†] Robert E. Mulvey,*[,†] Charles T. O'Hara,[†] John A. Parkinson,[†] and Duncan M. Tooke[‡]

Contribution from the Department of Pure and Applied Chemistry, University of Strathclyde, Glasgow G1 1XL, U.K., and School of Natural Sciences (Chemistry), University of Newcastle, Newcastle upon Tyne NE1 7RU, U.K.

Received May 12, 2004; E-mail: r.e.mulvey@strath.ac.uk

Abstract: Subjecting ferrocene, ruthenocene, or osmocene to the synergic amide base sodium−magnesium tris(diisopropylamido) affords a unique homologous series of metallocene derivatives of general formula $[\{M(C_5H_3)_2\}Na_4Mg_4(i\text{-}Pr_2N)_8]$ (where M = Fe (**1**), Ru (**2**), or Os (**3**)). X-ray crystallographic studies of **1**−**3** reveal a common molecular "inverse crown" structure comprising a 16-membered $[(NaNMgN)_4]^{4+}$ "host" ring and a metallocenetetraide $[M(C_5H_3)_2]^{4-}$ "guest" core, the cleaved protons of which are lost selectively from the 1, 1′, 3, and 3′-positions. Variable-temperature NMR spectroscopic studies indicate that **1**, **2**, and **3** each exist as two distinct interconverting conformers in arene solution, the rates of exchange of which have been calculated using coalescence and EXSY NMR measurements.

Introduction

The ability to metalate parent metallocene molecules is of fundamental importance to metallocene chemistry. Entry can be gained to a vast expanse of ring-substituted derivatives, compounds in demand across the borders of science, medicine, and technology, by exploiting the metal-activated offspring as synthetic intermediates.[1,2] Lithiation is the vehicle most often used in this endeavor.[3] Monolithioferrocene is accessible in high yield by reacting *tert*-butyllithium with ferrocene in THF solution.[4,5] When more than one hydrogen atom needs to be removed from the parent metallocene (or when starting from a prior-substituted metallocene), regioselective metalation is highly desirable. Dilithiation of ferrocene (predominately in the 1,1′-positions) can be accomplished by increasing the stoichiometry of the alkyllithium base in the presence of a chelating tertiary amine [TMEDA, $Me_2NCH_2CH_2NMe_2$, or PMDETA, $(Me_2NCH_2CH_2)_2NMe$]. While there is a general dearth of solid-state structures in the *s*-block metallocene area, both TMEDA[6] and PMDETA[7] complexes of dilithioferrocene have been crystallographically characterized. Higher lithiation (or polar metalation) of ferrocene represents a far greater challenge to synthetic chemists. Several strong metalating agents (for example, a 4- to 8-fold stoichiometric excess of *n*-BuLi,[8] the reactive alkylsodium *n*-PeNa,[9] or up to 20 molar equivalents of the alkylpotassium *n*-BuK[10]) have been reputed to bring about polydeprotonation of ferrocene (as determined indirectly by in situ electrophilic quenching protocols), but leading only in sporadic ways to complex mixtures of little practical use. In our contribution herein, we describe a new and effective polymetalation strategy illustrated through the synthesis of a remarkable homologous series of regioselectively tetrametalated group 8 metallocenes of general formula $[\{M(C_5H_3)_2\}Na_4Mg_4(i\text{-}Pr_2N)_8]$ (where M = Fe (**1**), Ru (**2**), or Os (**3**)). The ferrocenyl member **1** was the subject of a preliminary communication.[11] Here we add the ruthenocenyl **2** and osmocenyl **3** congeners, which, like **1**, have been made in isolable, pure crystalline forms that have permitted their crystallographic and spectroscopic (NMR) characterization.

Focusing further afield of metallocene chemistry, this trio of compounds represents the latest development in our ongoing investigations into the special synergic effects of mixed alkali metal−magnesium amide base systems.[12] In effecting depro-

[†] University of Strathclyde.
[‡] University of Newcastle.

(1) Togni, A.; Hayashi, T. *Ferrocenes*; VCH: Weinheim, Germany, **1995**.
(2) Long, N. J. *Metallocenes: An Introduction to Sandwich Compounds*, 1st ed.; Blackwell Science: Oxford, 1998.
(3) First report of ferrocene lithiation: Benkesser, R. A.; Goggin, D.; Scholl, G. *J. Am. Chem. Soc.* **1954**, *76*, 4025.
(4) Rebieré, F.; Samuel, O.; Kagan, H. B. *Tetrahedron Lett.* **1990**, *31*, 3121.
(5) High yields of lithioferrocene can also be obtained using an 8:1 *t*-BuLi:KO*t*-Bu superbasic mixture: Sanders, R.; Mueller-Westerhoff, U. T. *J. Organomet. Chem.* **1996**, *512*, 219.
(6) Butler, I. R.; Cullen, W. R.; Ni, J.; Rettig, S. J. *Organometallics* **1985**, *4*, 2196.
(7) Walczak, M.; Walczak, K.; Mink, R.; Rausch, M. D.; Stucky, G. D. *J. Am. Chem. Soc.* **1978**, *100*, 6382.
(8) Halasa, A. F.; Tate, D. P. *J. Organomet. Chem.* **1970**, *24*, 769.
(9) Post, E. W.; Crimmins, T. F. *J. Organomet. Chem.* **1978**, *161*, C17.
(10) Osbourne, A. G.; Whiteley, R. H. *J. Organomet. Chem.* **1978**, *162*, 79.
(11) Clegg, W.; Henderson, K. W.; Kennedy, A. R.; Mulvey, R. E.; O'Hara, C. T.; Rowlings, R. B.; Tooke, D. M. *Angew. Chem., Int. Ed.* **2001**, *40*, 3902.
(12) Mulvey, R. E. *Chem. Commun.* **2001**, 1049.

10.1021/ja0472230 CCC: $27.50

tonation, these heterometallic bases can generate novel macrocyclic structures in which a cationic ring of alternating metal and nitrogen atoms (the residue of the base) surrounds an anionic core (the deprotonated substrate). Though coined previously by other researchers in different contexts,[13−15] the term "inverse crown" seems particularly apt to describe this type of structure as its Lewis acidic (metal cation) and Lewis basic (substrate anion) sites have been interchanged relative to those in conventional crown ether complexes.

Results and Discussion

Synthesis. Previously we have demonstrated the unusual deprotonating ability that mixed sodium−magnesium tris(TMP) "NaMg(TMP)$_3$" (TMP = 2,2,6,6,-tetramethylpiperidide, Me$_2$C-(CH$_2$)$_3$C(Me)$_2$N) can display toward arene molecules. For example,[16] toluene can be selectively dideprotonated in ring sites (2,5-positions) without cleavage of a methyl hydrogen atom, as manifested in the 12-membered inverse crown ring system [Na$_4$Mg$_2$(TMP)$_6$(C$_6$H$_3$CH$_3$)] **4**. On the other hand, when the "NaMg(TMP)$_3$" synergic base was applied to ferrocene, the disodium−trimagnesium trinuclear ferrocenophane [{Fe(C$_5$H$_4$)$_2$}$_3$-{Na$_2$Mg$_3$(TMP)$_2$·(TMPH)$_2$}] **5** was produced.[17] Notwithstanding the product's odd stoichiometry and triferrocenyl constitution, its formation is less extraordinary from a deprotonation standpoint, as its ferrocene-1,1′-diyl units are the norm when ferrocene undergoes mainstream dimetalation (as encountered in the aforementioned TMEDA[6] and PMDETA[7] complexes).

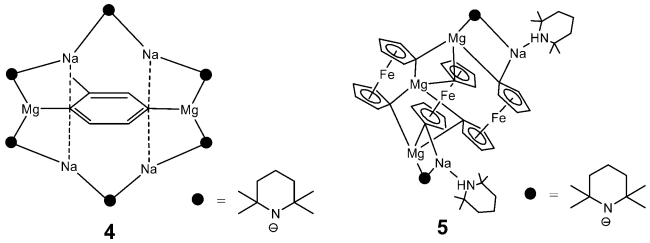

4

5

For that reason we turned our attention to another sterically demanding secondary amide that derived from diisopropylamine, *i*Pr$_2$N$^-$. The first step in the synthesis of **1**, **2**, and **3** was therefore to generate in situ the corresponding tris(diisopropylamide) "NaMg(*i*-Pr$_2$N)$_3$" by treating a 1:1 stoichiometric mixture of *n*-BuNa/*n*,*s*-Bu$_2$Mg (dibutylmagnesium, DBM) in aliphatic hydrocarbon solution with 3 molar equivalents of the amine. Next, the appropriate metallocene was introduced: several reaction stoichiometries were screened to reveal that optimum yields are obtained using only 0.25 molar equivalents (eq 1), commensurate with the stoichiometry of the desired product. In all cases, toluene was added to the concentrated reaction solution to aid crystallization of the product. Diagnostic of the successful metalation of ferrocene, the reaction solution turns from orange to red; no such color change accompanies the conversion of the larger metallocenes, the solutions of which remain yellow. The crystalline products show the same distinction, with the ferrocenyl complex being red, and the other complexes yellow (pale yellow in the case of **3**). To date, the best yields of crystalline material obtained have been 72, 53, and 62% for **1**, **2**, and **3**, respectively. Occasionally the reaction solutions can afford an oily residue in addition to and concomitant with a substantially lower yield of crystalline product. We suspect that this complication could be due to a problem with commercial DBM samples. Developed by FMC, DBM is not a precise stoichiometric compound but rather a solution mixture of *n*- and *s*-butyl groups (presumed to be in a 1:1 ratio) admixed with a much smaller proportion of *n*-octyl groups, introduced to aid solubility of the reagent in acyclic hydrocarbon solvents such as *n*-heptane. These bare compositional facts mask the inherent chemical complexity of the mixture. Given the propensity of organomagnesium compounds to self-aggregate and the ability of alkyl groups to act as bridges, it is possible that a plethora of species could be present in solution: likely constituents include *n*-Bu$_2$Mg, *s*-Bu$_2$Mg, *n*-Bu(*s*-Bu)Mg, and permutational oligomers such as [(*n*-Bu)$_x$(*s*-Bu)$_y$Mg$_{(x+y)/2}$] as well as a small concentration of *n*-Oct-containing isomers. As a consequence, ^{1}H NMR spectra of a sample of DBM in C$_6$D$_6$ solution recorded over a temperature range (300−360 K) are extremely complicated, showing signs of dynamic exchange processes.[18] However, while a complete interpretation of the alkyl region of the spectra (in this case, spanning approximately 2.0 to −1.0 ppm) is problematical, of greater diagnostic significance is the unexpected presence of a set of overlapping resonances outside of this fingerprint region (at approximately 4.0−3.6 ppm). These resonances can be assigned to adventitious butoxide groups (for example, *n*-BuO$^-$, *s*-BuO$^-$), further evidence for which comes from sister signals found in the corresponding ^{13}C NMR spectra at around 65 ppm (denoting −*C*H$_2$−O$^-$/−*C*H−O$^-$ carbon atoms). This contamination almost certainly arises from accidental exposure of the air-sensitive reagent to atmospheric oxygen, a common occurrence with polar organometallic compounds in general, though the associated chemistry is not all that well understood. Since alkoxides are generally much weaker bases than alkyls, the former will presumably remain in the reaction mixture following the amination step that is intended to produce pure "NaMg-(*i*-Pr$_2$N)$_3$".[19] Mixed alkoxo-amido adducts may possibly be involved at this stage. In that regard, it is significant that sodium−magnesium−alkoxide−diisopropylamide inverse crowns of general formula [{NaMg[*i*-Pr$_2$N]$_2$RO}$_2$] (where R = *n*-Bu or *n*-Oct), synthesized rationally by treating mixed-metal amide mixtures with the appropriate alcohol, have been reported, though these 2:1, amide/alkoxide adducts are crystalline compounds.[20] In our case, it appears that the unplanned participation of alkoxide groups (in lower, nonstoichiometric quantities)

(13) First use of the term "inverse crown": Stemmler, A. J.; Kampf, J. W.; Pecoraro, V. L. *Inorg. Chem.* **1995**, *34*, 2271.
(14) For the report of an "inverse crown" ether sandwich, see: Saalfrank, R. W.; Bernt, I.; Hampel, F.; Scheurer, A.; Nakajima, T.; Huma, S. H. Z.; Heinemann, F. W.; Schmidtmann, M.; Muller, A. *Polyhedron* **2003**, *22*, 2985.
(15) For key references to "anti-crown" mercuracarborane complexes, see: (a) Badr, I. H. A.; Diaz, M.; Hawthorne, M. F.; Bachas, L. G. *Anal. Chem.* **1999**, *71*, 1371. (b) Lee, H.; Knobler, C. B.; Hawthorne, M. F. *J. Am. Chem. Soc.* **2001**, *123*, 8543. (c) Zheng, Z. P.; Knobler, C. B.; Mortimer, M. D.; Kong, G. G.; Hawthorne, M. F. *Inorg. Chem.* **1996**, *35*, 1235. (d) For a review, see: Wedge, T. J.; Hawthorne, M. F. *Coord. Chem. Rev.* **2003**, *240*, 111.
(16) Kennedy, A. R.; Mulvey, R. E.; Rowlings, R. B. *Angew. Chem., Int. Ed.* **1998**, *37*, 3180.
(17) Henderson, K. W.; Kennedy, A. R.; Mulvey, R. E.; O'Hara, C. T.; Rowlings, R. B. *Chem. Commun.* **2001**, 1678.
(18) See Experimental Section.
(19) TMEDA-solvated "NaMg(*i*-Pr$_2$N)$_3$" has recently been prepared: Hevia, E.; Kenley, F. R.; Kennedy, A. R.; Mulvey, R. E.; Rowlings, R. B. *Eur. J. Inorg. Chem.* **2003**, 3347.
(20) Drewette, K. J.; Henderson, K. W.; Kennedy, A. R.; Mulvey, R. E.; O'Hara, C. T.; Rowlings, R. B. *Chem. Commun.* **2002**, 1176.

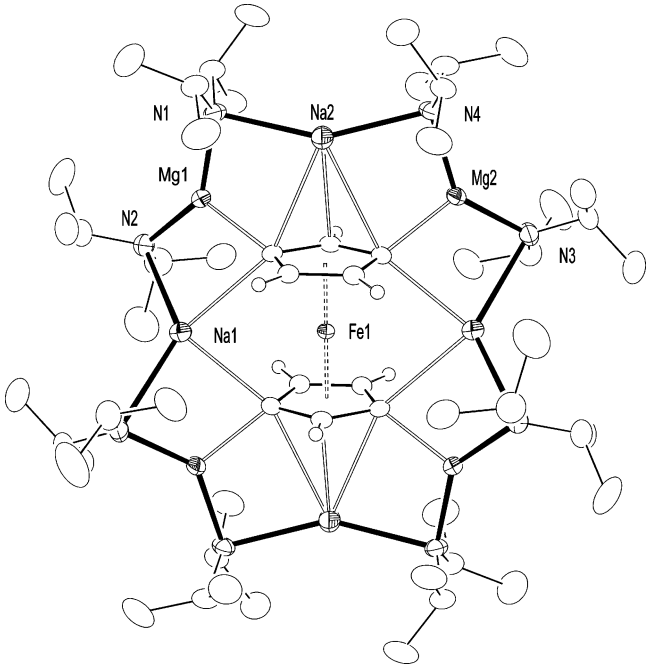

Figure 1. Molecular structure of **1** showing selected atom labeling. Hydrogen atoms, except those belonging to the C_5H_3 rings, have been omitted for clarity, and ellipsoids are at the 50% probability level.

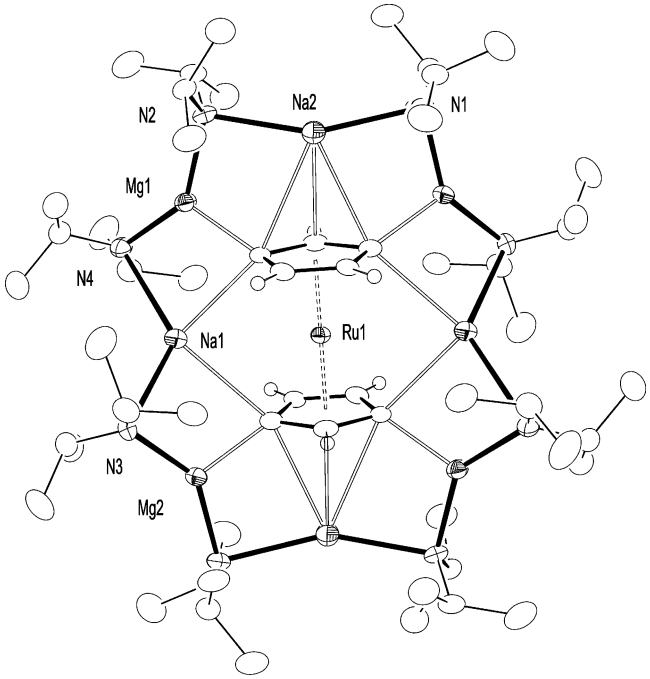

Figure 2. Molecular structure of **2** showing selected atom labeling. Hydrogen atoms, except those belonging to the C_5H_3 rings, have been omitted for clarity, and ellipsoids are at the 50% probability level.

causes the reaction solutions of **1**, **2**, and **3** to partially degrade to an oil-like substance.

$$4\ n\text{-BuNa} + 4\ n,s\text{-Bu}_2\text{Mg} + 12\ i\text{-Pr}_2\text{NH} + \text{M}(\text{C}_5\text{H}_5)_2 \rightarrow [\{\text{M}(\text{C}_5\text{H}_3)_2\}\text{Na}_4\text{Mg}_4(i\text{-Pr}_2\text{N})_8] + 12\ \text{BuH} + 4\ i\text{-Pr}_2\text{NH} \quad (1)$$

where M = Fe, Ru, or Os.

New Inverse Crown Architecture. Crystal structure determinations of **1**, **2**, and **3** reveal a common centrosymmetric molecular structure. This commonality is clearly evident from the individual structures shown in Figures 1−3, respectively.

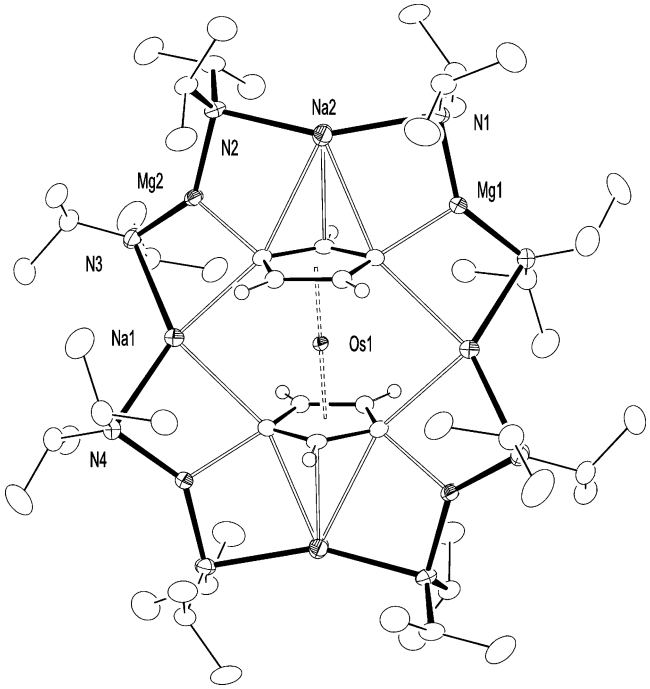

Figure 3. Molecular structure of **3** showing selected atom labeling. Hydrogen atoms, except those belonging to the C_5H_3 rings, have been omitted for clarity, and ellipsoids are at the 50% probability level.

Keeping to the inverse crown interpretation, the common structure can be regarded formally as a host−guest assembly of a 16-membered $[(NaNMgN)_4]^{4+}$ ring with a metallocenyl $[M(C_5H_3)_2]^{4-}$ center. Protons have been cleaved from the 1, 1′, 3, and 3′-positions of the parent metallocene (a fact corroborated by the NMR spectroscopic study, vide infra), associated with carbon atoms C27, C27*, C29, and C29*. Within the host ring, the metal atoms linked by the N bridges are alternately sodium and magnesium. There are two chemically distinct types of sodium atom: part of the linear Na···Fe···Na arrangement that bisects the metallocenyl fragment, Na1 occupies a μ_2-bonding site between the Cp′ rings (Cp′ = C_5H_3) and completes its distorted tetrahedral coordination by binding to two N atoms; in contrast, Na2 engages with the π-face of the Cp′ ring in an asymmetrical η^3-fashion and completes a pseudo-trigonal coordination (counting the Cp′ ring as a single coordination point) by also binding to a pair of N atoms. Formally refilling the positions left vacant by the cleaved hydrogen atoms, the four chemically equivalent magnesium atoms (arranged in two crystallographically distinct pairs) adopt a distorted trigonal planar coordination of one carbon and two nitrogen atoms.

Existing in two chemically inequivalent sets comprising N1/N4 and N2/N3, all eight amido N atoms display distorted tetrahedral geometries. Their geminal *i*-Pr substituents twist out of each other's way to minimize Me···Me repulsions, a phenomenon seemingly maintained in solution (vide infra). To facilitate the anchoring of the dideprotonated edge of each Cp′ ring, the 16-membered azaheterobimetallic ring must pucker severely in a "Z-shaped" conformation, defined by sections N2Mg1N1Na2N4Mg2N3, N2Na1N3′···N2′Na1′N3, and N2′Mg1′N1′Na2′N4′Mg2′N3′ (Figure 4). The Cp′ rings themselves lie parallel and staggered relative to one another (a key factor in the C_i symmetry of the whole molecule), and there is essentially no ring slippage.

Table 1. Key Corresponding Bond Distances within Complexes **1**, **2**, and **3**

bond distances (Å)	**1** M = Fe	**2** M = Ru	**3** M = Os	bond distances (Å)	**1** M = Fe	**2** M = Ru	**3** M = Os
Mg1−N1	2.0397(13)	2.044(3)	2.0379(13)	Na2···C26	3.256(2)	3.345(3)	3.352(2)
Mg1−N2	2.0163(14)	2.014(3)	2.0133(14)	Na2−C27	2.8329(15)	2.857(3)	2.8470(16)
Mg2−N3	1.9965(13)	1.997(3)	1.9965(13)	Na2−C28	2.6080(15)	2.595(3)	2.5887(15)
Mg2−N4	2.0411(13)	2.047(3)	2.0457(13)	Na2−C29	2.9232(15)	2.966(3)	2.9597(16)
Mg1−C27	2.1469(15)	2.136(3)	2.1347(15)	mean Na1···M	3.286	3.223	3.223
Mg2−C29	2.1580(15)	2.150(3)	2.1458(15)	Na1···Na1′	6.572	6.459	6.447
Na1−N2	2.5347(15)	2.542(3)	2.5467(14)	Na2···Na2′	8.663	9.014	9.003
Na1−N3′	2.7113(15)	2.737(3)	2.7359(15)	C25−C26	1.430(2)	1.420(4)	1.439(2)
Na2−N1	2.5068(14)	2.511(3)	2.5120(14)	C25−C27	1.434(2)	1.434(4)	1.443(2)
Na2−N4	2.4661(14)	2.475(3)	2.4709(14)	C26−C29	1.438(2)	1.435(4)	1.444(2)
Na1−C27	2.7546(16)	2.818(3)	2.8157(16)	C27−C28	1.459(2)	1.458(4)	1.464(2)
Na1−C29′	2.6287(15)	2.661(3)	2.6574(16)	C28−C29	1.454(2)	1.453(4)	1.463(2)
Na2···C25	3.201(2)	3.286(3)	3.292(2)				

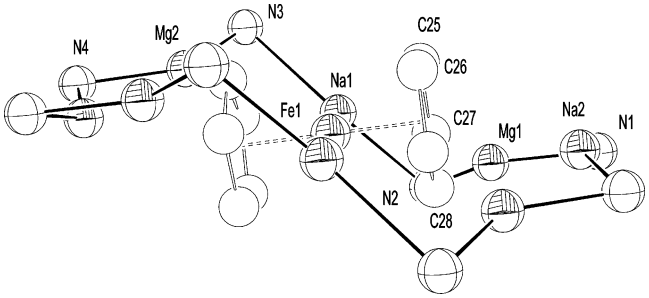

Figure 4. Alternative side view of the common structure of **1**−**3** highlighting the pseudo-Z conformation of the azametalla host ring.

Table 2. Key Corresponding Bond Angles within Complexes **1**, **2**, and **3**

bond angles (deg)	**1**	**2**	**3**
Mg1−N1−Na2	90.84(5)	91.87(9)	92.03(5)
Mg1−N2−Na1	83.43(5)	85.65(9)	85.42(5)
Mg2−N3−Na1′	78.35(5)	79.83(9)	79.78(5)
Mg2−N4−Na2	93.70(5)	95.12(10)	95.17(5)
N2−Na1−N3	129.46(5)	128.61(9)	128.52(5)
C27−Na1−C29′	79.78(5)	85.89(9)	86.24(5)
N1−Na2−N4	150.43(5)	153.71(9)	153.76(6)
N1−Mg1−N2	140.40(6)	141.54(11)	141.63(6)
N1−Mg1−C27	112.09(9)	111.83(11)	111.96(6)
N2−Mg1−C27	107.49(9)	106.63(11)	106.40(6)
N3−Mg2−N4	136.70(6)	137.94(11)	138.25(6)
N3−Mg2−C29	116.14(9)	115.62(11)	115.60(6)
N4−Mg2−C29	107.15(9)	106.44(11)	106.15(6)
180−(Mg1−C27−centroid)	28.40	27.10	25.83
180−(Mg2−C29−centroid)	32.87	31.60	31.43

A salient feature emerging from the dimensions across the series **1**−**3** (selected bond lengths in Table 1; selected bond angles in Table 2) is that the host ring can accommodate any of the three different metallocene molecules without significant alteration to its constituent bond lengths or bond angles. The striking similarity of the corresponding dimensions of these 16-membered rings is evident from the restricted range of mean Mg−N bond lengths within **1**−**3** (2.016−2.018 Å), a statistic echoed in the Na−N data (2.555−2.566 Å). Interestingly, these values also show little variation from those in the previously reported diisopropylamide-based alkoxo[20] and hydrido[21] inverse crowns [{NaMg[*i*-Pr$_2$N]$_2$*n*-BuO}$_2$] and [{NaMg[*i*-Pr$_2$N]$_2$(μ-H).-(toluene)}$_2$], respectively, (Mg−N bond lengths 2.051 Å (mean) and 2.065 (18) Å, respectively; Na−N bond lengths, 2.469 Å (mean) and 2.4807(18) Å, respectively), which, it should be stressed, are in contrast to smaller eight-membered ring compounds. It can be reasoned from this comparison that the flexibility of the "[(NaNMgN)$^+$]$_n$" system (where N = *i*-Pr$_2$N) to encapsulate guests of different chemical composition and size (including a series of metallocenes, alkoxides, and hydride) stems not from microscopic bond length adjustments but from a macroscopic, chameleonic ability to change aggregation state (i.e., n = 4 in **1**−**3**, cf., n = 2 in the alkoxide and hydride structures).

This picture could prompt a comparison with the "conveyor-belt" mechanism[22] proposed to exist when lithium diisopropylamide functions as a base. However, in that case, the building up of molecular lithium amide units to fit a specific metalation task represents a pre-metalation event, whereas here inverse crown ring aggregates are products of post-metalation. As yet, it is not clear whether synergic amide-induced polymetalation is achieved by a single templating aggregate (à la conveyor belt model) made up of several active base sites or by multiple equivalents of the same base. Turning to angular dimensions within **1**−**3**, there is also close agreement between corresponding metal−N−metal bond angles and between corresponding N−metal−N bond angles, both of which come in four distinct sets: the former Mg1−N1−Na2, Mg1−N2−Na1, Mg2−N3−Na1′, and Mg2−N4−Na2 differ by only 1.19°, 2.22°, 1.48°, and 1.47°, respectively, across the series; and the latter N2−Na1−N3, N1−Na2−N4, N1−Mg1−N2, and N3−Mg2−N4 differ by only 0.94°, 3.33°, 1.23°, and 1.55°, respectively. across the series. Note that the bond angles subtended at N in this list represent endocyclic ones, whereas those subtended at metal centers represent exocyclic ones. This pattern accounts for the directional Lewis acidity of the host ring, with available metal orbitals projecting inward toward the Lewis basic guest. It is significant that the largest difference in the aforementioned N−metal−N bond angles is that for N1−Na2−N4. This reflects the pushing out of the pseudoaxial Na2 atoms as the host ring stretches to accommodate the taller 4d and 5d metallocenes, a point confirmed by comparison of the respective Na2···Na2′ separation distances for **1**, **2**, and **3** (8.663, 9.014, and 9.003 Å). In contrast to this vertical stretch, to counterbalance the greater Cp′···Cp′ separation distances in **2** and **3** (3.644 and 3.646 Å, respectively, cf., 3.354 Å in **1**), a horizontal contraction occurs in the pseudoequatorial Na1···Na1′ vector (6.572, 6.459, and 6.447 Å, for **1**, **2**, and **3,** respectively), though the extent of change (mean, 0.119 Å) is less marked (mean vertical difference, 0.345 Å). This horizontal contraction is not enough to prevent

(21) Gallagher, D. J.; Henderson, K. W.; Kennedy, A. R.; Mulvey, R. E.; O'Hara, C. T.; Rowlings, R. B. *Chem. Commun.* **2002**, 376.

(22) *Organometallics in Synthesis: A Manual*, 2nd ed.; Schlosser, M., Ed.; Wiley & Sons: Chichester, U.K., **2002**, p 32.

a significant elongation in the Na1−C27 and Na1−C29 bond lengths of **2** and **3** (by mean values of 0.063 and 0.032 Å, respectively, compared to those for **1**), which is accompanied by a widening of the Na···Cp′/Cp′ bond angles (mean for **2** and **3**, 86.07°; cf., 79.78(5)° for **1**). Emphasising the dominance of the Mg atoms within the host−guest bonding, there is decidedly less spread in the Mg−C bond lengths and N−Mg−C bond angles across the series (largest differences, 0.0122 Å and 1.09°, respectively). However, unlike in the toluene-based inverse crown **4**, the Mg atoms in **1**−**3** do not lie coplanar with the plane of the aromatic ring, but protrude out of it by 1.141(3)/0.981(3), 1.082(5)/0.876(5), and 1.071(3)/0.875(3) Å, respectively, for the two independent Mg−C bonds in each compound.[23] The bridge span may be an important consideration in this distinction, as in **4** the Mg atoms are joined by five-membered N−Na−N−Na−N arrangements, whereas here they are joined by a three-membered N−Na−N bridge. Presumably the latter setup offers less flexibility, and ring closure can be achieved only at the expense of a modest compromise to the σ-component of the Mg−C bonding. Turning to C−C bond lengths within the Cp′ rings, a consistent pattern across the series is evident, though the differences involved are rather modest: the nonmetalated edge (C25−C26) has the shortest (1.430(2), 1.420(4), and 1.439(2) Å for **1**−**3**, respectively), the 2-fold-metalated triatomic edge (C27−C28−C29) has the longest (mean values, 1.456, 1.456, and 1.464 Å, respectively), while the remaining singly metalated edges (C25−C29/C26−C27) have intermediate values (mean, 1.436, 1.435, and 1.444 Å, respectively).

Despite the vast mountain of literature on ferrocene (and metallocene) chemistry in general, the novelty of the structures of **1**−**3** is such that no direct comparisons, and very few tenuous comparisons, are available. Thus, searching the Cambridge Structural Database[24] revealed no hits for heterometallic sodium−magnesium (with the exception of the ferrocenophane species **5**) or homometallic sodium group 8 metallocene species. It follows that **1**−**3** exhibit the first structurally authenticated Na−metallocenyl bonds of this group. Only one previous article reporting homometallic magnesoferrocene structures was found,[25] though the compounds involved were not synthesized by direct magnesiation but by metathesis from a lithioferrocene and a magnesium halide. Representative of these compounds, [$(FcN)_2$Mg.THF] (where FcNH is dimethylaminomethylferrocene) is mononuclear with Mg bonded to both ferrocenyl units via the anionic C atoms adjacent to the alkyl-substituted position, to both *N*Me_2 atoms and to the O atom of THF. Less sterically shielded than those in **1**−**3** in accord with its higher five-coordinate environment, this Mg atom approaches the Cp plane more closely, implying a greater degree of σ-character in the Mg−C bonding. However, this more favorable directionality does not translate into shorter Mg−C bonds, as their mean length (2.156 Å) is essentially equivalent to that in **1** (2.152 Å), though the comparison is complicated by the lower coordination number (three) of the Mg atoms in **1**. For lithium, the crystal structures of two ferrocenophane species akin to **5** and a related uranium (IV) complex[26] [$\{Fe(C_5H_4)_2\}_3ULi_2$.(pyridine)$_3$] have been reported, in addition to the previously mentioned dilithioferrocene TMEDA[6] and PMDETA[7] complexes. To the best of our knowledge, no other directly *s*-block C-metalated ferrocenes (or ruthenocenes or osmocenes) have been crystallographically characterized. The structural literature on other metal and metalloidal derivatives of ferrocene is far less impoverished, including examples where Al,[27] Ga,[28] Ge,[29] Hg,[30] Pt,[31] Sn,[32] Ti,[33] V,[34] W,[35] or Zr[36] are directly attached to the carbon framework of the sandwich compound. The most pertinent example is that of 1,1′,3,3′-tetrakis(trimethylstannyl)ferrocene,[37] which, in contrast to **1**−**3**, is not made by direct metalation of the parent metallocene but by a sequential strategy from stannyl-substituted monocyclopentadiene precursors. Metalated ruthenocene structures are much rarer, with examples limited to the soft metals Pt[38] and Au.[39] At the time of this writing, **3** represents the sole example of a metalated osmocene structure.

Solution Behavior. Good solubility of **1**−**3** in arene solvents has permitted detailed NMR spectroscopic studies to be carried out. The spectra obtained are generally similar for each compound, suggesting that the structural resemblance between the three compounds seen in the crystalline state is maintained in arene solution. There are three distinct diagnostic regions within the ^{1}H NMR spectra: from low to high frequency, these are populated by CH_3, *i*-Pr C*H*, and Cp′ C*H* resonances, as shown in the representative spectrum of the osmocenyl inverse crown **3** in C_6D_6 solution (Figure 5).

Most informative is the last set of resonances, as it establishes the presence of two distinct species that further experiments indicate are two interconverting conformations of the ring structure observed in the solid state. For **3**, the major conformer exhibits a doublet at 4.56 ppm and a triplet at 3.77 ppm (for which $^4J(^1H,^1H) = 0.62$ Hz is common) and the minor conformer exhibits corresponding resonances and couplings at 4.52 and 3.85 ppm, with the conformers in an approximate ratio of 3:1. Using the crystal structure notation, we can assign the doublets and triplets to H atoms attached to C25/C26 and C28, respectively. In the case of **2**, the corresponding pairs of resonances appear at 4.45/3.68 ppm (major conformer) and 4.41/3.73 ppm (minor conformer), and the major/minor conformer

(23) In the preliminary communication, we inadvertently stated incorrectly that the Mg centers protrude out of the aromatic plane by 58.4° and 63.1°.
(24) (a) Allen, F. H. *Acta Crystallogr., Sect. B* **2002**, *58*, 380. (b) Cambridge Structural Database, Version 5.25 with January 2004 update.
(25) Seidel, N.; Jacob, K.; Fischer, A. K.; Pietzsch, C.; Zanello, P.; Fontani, M. *Eur. J. Inorg. Chem.* **2001**, 145.
(26) Bucaille, A.; Le Borgne, T.; Ephritikhine, M. *Organometallics* **2000**, *19*, 4912.
(27) For example, see: Knabel, K.; Krossing, I.; Nöth, H.; Schwenk-Kircher, H.; Schmidt-Amelunxen, M.; Seifert, T. *Eur. J. Inorg. Chem.* **1998**, 1095.
(28) For example, see: Jutzi, P.; Lenze, N.; Neumann, B.; Stammler, H.-G. *Angew. Chem., Int. Ed.* **2001**, *40*, 1424 and references therein.
(29) For example, see: Castruita, M.; Cervantes-Lee, F.; Mahmoud, J. S.; Zhang, Y.; Pannell, K. H. *J. Organomet. Chem.* **2001**, *637*, 664.
(30) For example, see: Sunkel, K.; Kiessling, T. *J. Organomet. Chem.* **2001**, *637*, 796.
(31) For example, see: Yoshida, T.; Tanaka, S.; Adachi, T.; Yoshida, T.; Onitsuka, K.; Sonogashira, K. *Angew. Chem., Int. Ed. Engl.* **1995**, *34*, 319.
(32) For examples, see: (a) Jäkle, F.; Rulkens, R.; Zech, G.; Foucher, D. A.; Lough, A. J.; Manners, I. *Chem.−Eur. J.* **1998**, *4*, 2117. (b) Herberhold, M.; Steffl, U.; Milius, W.; Wrackmeyer, B. *Angew. Chem., Int. Ed. Engl.* **1996**, *35*, 1803.
(33) For example, see: Zakharova, L. N.; Struchkov, Y. T.; Sharutin, V. V.; Suvorova, O. N. *Cryst. Struct. Commun.* **1979**, *8*, 439.
(34) Kohler, F. H.; Geike, W. A.; Hofmann, P.; Schubert, U.; Stauffert, P. *Chem. Ber.* **1984**, *117*, 904.
(35) Herberhold, M.; Kniesel, H.; Haumaier, L.; Gieren, A.; Ruiz-Perez, C. *Z. Naturforsch., B: Chem. Sci.* **1996**, *41*, 1431.
(36) Broussier, R.; Da Rold, A.; Gautheron, B.; Dromzee, Y.; Jeannin, Y. *Inorg. Chem.* **1990**, *29*, 1817.
(37) Lenze, N.; Neumann, B.; Salmon, A.; Stammler, A.; Stammler, H.-G.; Jutzi, P. *J. Organomet. Chem.* **2001**, *619*, 74.
(38) Yoshida, T.; Shinohara, T.; Onitsuka, K.; Ozawa, F.; Sonogashira, K. *J. Organomet. Chem.* **1999**, *574*, 66.
(39) Nefedova, M. N.; Mamed'yarova, I. A.; Sokolov, V. I.; Smyslova, E. I.; Kuz'mina, L. G.; Grandberg, K. I. *Russ. Chem. Bull.* **1994**, 1335.

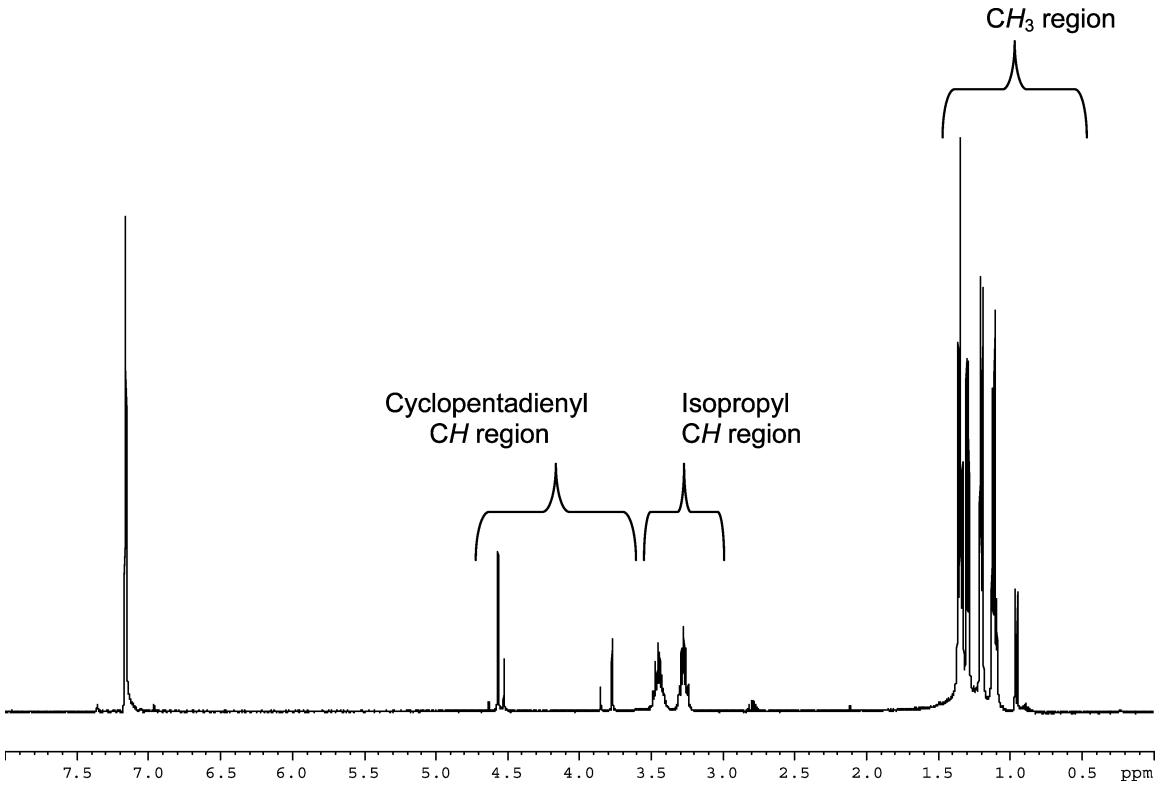

Figure 5. ^{1}H NMR spectrum of a deuteriobenzene solution of **3** recorded at ambient temperature.

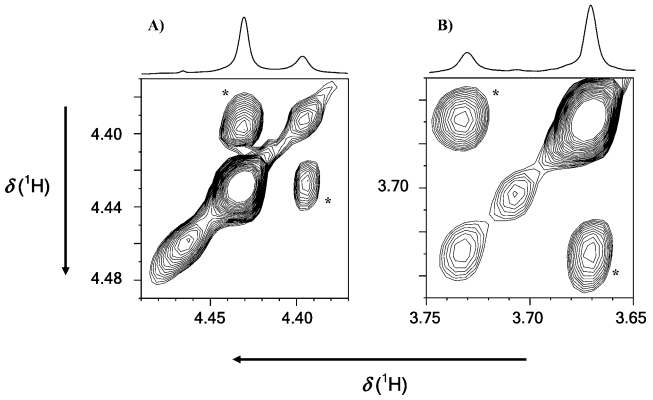

Figure 6. Key regions of the 500 ms 2D [^{1}H, ^{1}H] EXSY NMR spectrum of **2** acquired at 9.4 T (320 K) showing the presence of two interconverting structures: (A) H25/H26 resonance region and (B) H28 resonance region. For both regions, cross-peaks due to the presence of the slow (on the NMR time scale) chemical exchange process are indicated by *****. For each region, the 1D ^{1}H NMR spectrum of **2** (at 320 K) is shown at the top of each section of 2D data.

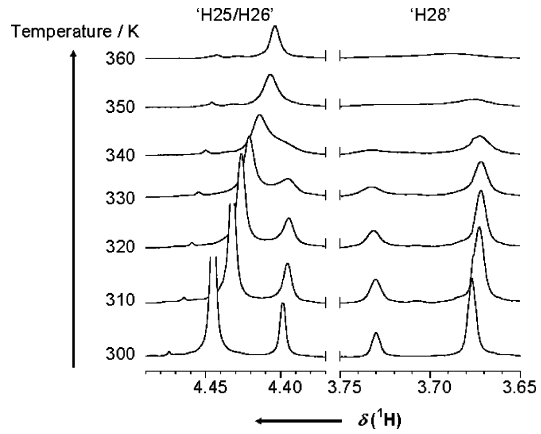

Figure 7. Variable-temperature ^{1}H NMR spectra of a deuteriotoluene solution of **2** recorded over the range 300−360 K.

ratio is again approximately 3:1. The situation with **1** is different in that the distinct conformers exist in an equal 1:1 population ratio, but the same pattern of resonances is present (doublet at 4.22 ppm, triplet at 3.50 ppm; doublet at 4.21 ppm, triplet at 3.55 ppm; note that the resonance at 3.50 ppm was inadvertently missed in the preliminary report of **1** as it is obscured by an overlapping *i*-Pr C*H* resonance). Comparing these Cp′ *H* resonances, it is discernible that corresponding ones shift to higher frequency in concert with an increase in the period (3d, 4d, 5d) of the transition metal involved, thus mimicking the trend observed in the ^{1}H NMR spectra of the parent metallocenes.[40] The methyl region of the ^{1}H NMR spectra of **1**−**3** is more complicated, comprising a series of overlapping doublets, which, in the cases of **2** and **3**, are divided into two equal sets of relative integral 3:1 commensurate with the ratio of conformers. This complexity reflects the eight chemically inequivalent Me groups, four per unique conformer, that would be expected from a structure in solution matching the crystalline structure. ^{13}C NMR spectroscopic data support this assignment, as eight separate methyl *C* resonances are clearly visible in the spectra of **1**−**3**. 2D[^{1}H, ^{1}H] EXSY NMR data (Figure 6 depicts those of **2**) establish that a slow exchange takes place between the two conformers in each solution. Exchange rates at 300 K are calculated to be 0.4 ± 0.1 s^{-1} (forward and reverse have same rate, therefore have a 50:50 mix) for **1**; 0.32 ± 0.04 s^{-1} (minor to major) and 0.12 ± 0.01 s^{-1} (major to minor) for **2**; and 0.45 ± 0.05 s^{-1} (minor to major) and 0.16 ± 0.02 s^{-1} (major to minor) for **3**.

(40) The chemical shifts for the parent metallocenes (in C_6D_6) are δ 4.00, 4.47, and 4.63 ppm, respectively, for ferrocene, ruthenocene, and osmocene.

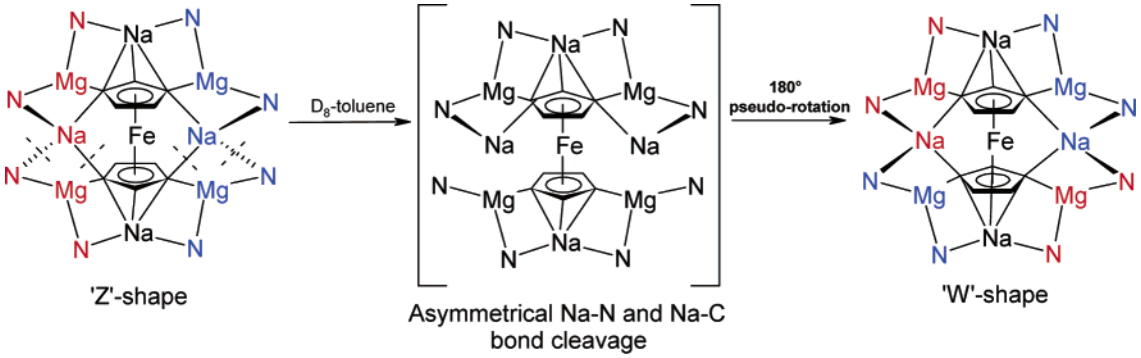

Figure 8. Proposed interconversion between the postulated conformers.

This fluxionality is corroborated by variable-temperature ^{1}H NMR spectra (those of **2** recorded over the range 300−360 K are reproduced in Figure 7). The respective coalescence temperatures for **1**, **2**, and **3** were found to be 370, 350, and 355 K. Logic dictates that one conformer must correspond to the pseudo-C_i molecule of the crystal structure, which displays staggered Cp′ ligands. As yet the identity of the second conformer is not known for certain, though it is possible that it could be a C_2 alternative with eclipsed as opposed to staggered Cp′ ligands. The interconversion between the two conformers could be achieved by formally breaking weak electrostatic links to the equatorial Na atoms and rotating one half of the molecule by 180° about the centroid···M···centroid axis, to give the host ring more of a "W" shape than a "Z" shape (Figure 8). It is also plausible that the exchange phenomenon that is observed may be due to rearrangement of Cp/Cp′ ligands, or it may be as a consequence of a change in the geometry of the host ring alone through flipping and/or locking of the diisopropylamido side chains.

Thus, it seemed appropriate to investigate by DFT[41,42] calculations the feasibility of the presence of a C_2 sister conformer to **1**. The geometry optimization procedures were performed using the Gaussian 03 computer program[43] employing the B3LYP[44−46] density functional method and the 6-31G* basis set.[47−49] The C_i version (**I**) of **1** was modeled initially, and then the C_2 variation (**II**) was constructed by the aforementioned interconversion scheme (in Figures 9 and 10, the side view along the Na(1)···Fe···Na(1) line axis is shown, illustrating the structural relationship between the two models). No theoretical simplification of the models was carried out, so both **I** and **II** have the same molecular formula as **1**, [{Fe(C_5H_3)$_2$}Na_4Mg_4-(*i*-Pr_2N)$_8$]. It was found that the energy difference between the two models was 5.4 kcal mol^{-1}, with model **I** having the lower energy.[50] This energy differential is small enough to suggest that, in the presence of arene solvents, the C_2 variant is a distinct possibility as the second conformer.

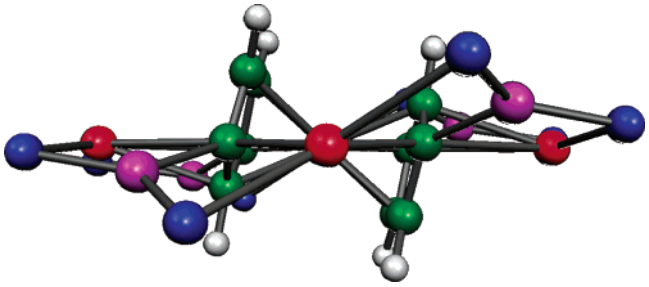

Figure 9. Side view of model **I** along the Na(1)···Fe···Na(1) axis. Color code: red, Na; green, C; blue, N; magenta, Mg; white, H.

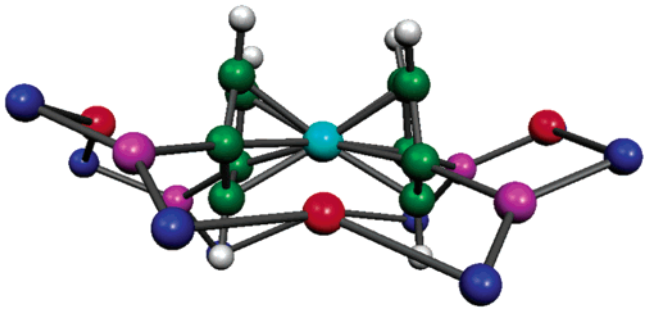

Figure 10. Side view of model **II**, emphasising the W-shape of the host ring. Color code: red, Na; green, C; blue, N; magenta, Mg; white, H; cyan, Fe.

The calculated bond lengths of models **I** and **II** are given in Table 3, along with the relevant experimental values taken from the X-ray determination of **1**. In general, the key structural dimensions calculated for model **I** agree favorably with those found in the solid-state structure of **1**.[51] This is especially true within the ferrocene ring unit, where the discrepancy is less than 0.01 Å. It is also evident that the comparable bond distances in models **I** and **II** are similar, suggesting that, on changing the molecule from C_i to C_2 symmetry, relatively little structural

(41) Hohenberg, P.; Kohn, W. *Phys. Rev.* **1964**, *136*, B864.
(42) Kohn W.; Sham, L. J. *Phys. Rev.* **1965**, *140*, A1133.
(43) Frisch, M. J.; Trucks, G. W.; Schlegel, H. B.; Scuseria, G. E.; Robb, M. A.; Cheeseman, J. R.; Montgomery, J. A., Jr.; Vreven, T.; Kudin, K. N.; Burant, J. C.; Millam, J. M.; Iyengar, S. S.; Tomasi, J.; Barone, V.; Mennucci, B.; Cossi, M.; Scalmani, G.; Rega, N.; Petersson, G. A.; Nakatsuji, H.; Hada, M.; Ehara, M.; Toyota, K.; Fukuda, R.; Hasegawa, J.; Ishida, M.; Nakajima, T.; Honda, Y.; Kitao, O.; Nakai, H.; Klene, M.; Li, X.; Knox, J. E.; Hratchian, H. P.; Cross, J. B.; Adamo, C.; Jaramillo, J.; Gomperts, R.; Stratmann, R. E.; Yazyev, O.; Austin, A. J.; Cammi, R.; Pomelli, C.; Ochterski, J. W.; Ayala, P. Y.; Morokuma, K.; Voth, G. A.; Salvador, P.; Dannenberg, J. J.; Zakrzewski, V. G.; Dapprich, S.; Daniels, A. D.; Strain, M. C.; Farkas, O.; Malick, D. K.; Rabuck, A. D.; Raghavachari, K.; Foresman, J. B.; Ortiz, J. V.; Cui, Q.; Baboul, A. G.; Clifford, S.; Cioslowski, J.; Stefanov, B. B.; Liu, G.; Liashenko, A.; Piskorz, P.; Komaromi, I.; Martin, R. L.; Fox, D. J.; Keith, T.; Al-Laham, M. A.; Peng, C. Y.; Nanayakkara, A.; Challacombe, M.; Gill, P. M. W.; Johnson, B.; Chen, W.; Wong, M. W.; Gonzalez, C.; Pople, J. A. *Gaussian 03*, revision A.1; Gaussian, Inc.: Pittsburgh, PA, 2003.
(44) Becke, A. D. *J. Chem. Phys.* **1993**, *98*, 5648.
(45) Lee, C.; Yang, W.; Parr, R. G. *Phys. Rev.* **1988** *37*, B785.
(46) Miehlich, B.; Savin, A.; Stoll, H.; Preuss, H. *Chem. Phys. Lett.* **1989**, *157*, 200.
(47) Ditchfield, R.; Hehre, W. J.; Pople, J. A. *J. Chem. Phys.* **1971**, *54*, 724.
(48) Hehre, W. J.; Ditchfield, R.; Pople, J. A. *J. Chem. Phys.* **1972**, *56*, 2257.
(49) Rassolov, V. A.; Pople, J. A.; Ratner, M. A.; Windus, T. L. *J. Chem. Phys.* **1998**, *109*, 1223.

(50) The total energies of model **I** and model **II** are −5432.772701 au and −5432.764129 au, respectively.
(51) It can be seen that there is reasonable agreement between the calculated and experimental bond distances. For the whole molecule, the average bond distance error is 0.034 Å and the average percentage error is 1.37%.

Table 3. Comparison of the Calculated Bond Distances for Models I and II with Those from the X-ray Crystallographic Data

bond	model **I** (C_i) (Å)	model **II** (C_2) (Å)	X-ray (**1**) (Å)	bond	model **I** (C_i) (Å)	model **II** (C_2) (Å)	X-ray (**1**) (Å)
Mg1−N1	2.088	2.087	2.040	Na2−C28	2.587	2.781	2.608
Mg1−N2	2.045	2.061	2.016	Na2−C29	2.877	2.880	2.923
Mg2−N3	2.058	2.037	1.997	Na1−Fe	3.356	3.389	3.286
Mg2−N4	2.071	2.086	2.041	C25−C26	1.431	1.435	1.430
Mg1−C27	2.167	2.174	2.147	C25−C27	1.443	1.447	1.434
Mg2−C29	2.168	2.164	2.158	C26−C29	1.442	1.446	1.438
Na1−N2	2.642	2.558	2.535	C27−C28	1.458	1.458	1.459
Na1−N3	2.564	2.704	2.711	C28−C29	1.459	1.457	1.454
Na2−N1	2.438	2.549	2.507	Fe−C25	2.066	2.035	2.063
Na2−N4	2.465	2.493	2.466	Fe−C26	2.066	2.029	2.065
Na1−C27	2.740	2.819	2.755	Fe−C27	2.118	2.121	2.112
Na1−C29	2.758	2.721	2.629	Fe−C28	2.036	2.070	2.031
Na2−C27	2.875	2.775	2.833	Fe−C29	2.117	2.123	2.118

perturbation of the cationic heterobimetallic amide ring is necessary. The main structural rearrangement (Figure 8) occurs in the metallocenyl fragment. In model **I**, the Cp′ rings are perfectly staggered as a consequence of the C_i symmetry of **1**; however, in model **II** the Cp′ rings lie in an almost eclipsed configuration with the R−C···C−R (where R = H or Na) dihedral angles ranging from 9.0° to 14.8°. The Cp′ rings in model **II** are not parallel with respect to each other. Instead they are tilted so that the atoms of the equivalent nonmetalated edges (i.e., C25 and C26) lie close together (3.158 Å), while the corresponding C28 atoms lie further apart (3.550 Å). Turning to the calculated bond angles, the most noteworthy change is for the Na(1)···Fe···Na(1) angle, which was 180° in model **I** and is 134.6° in model **II**. This change allows these Na atoms to maintain a comparable local bonding environment to that in model **I**.

Experimental Section

General Methods. ^{1}H and ^{13}C NMR spectra were recorded on a Bruker DPX 400 MHz or a Bruker AMX 400 MHz spectrometer. All ^{13}C NMR spectra were proton-decoupled. Exchange rates were calculated from EXSY NMR data on the basis of a two-site exchange process using the program D2DNMR.[52] Toluene and hexane were distilled from sodium−benzophenone. Ferrocene (Aldrich and Lancaster) was purified by recrystallizing from hexane. Ruthenocene (Aldrich) and osmocene (Strem) were used as received. *n*,*s*-Dibutylmagnesium in heptane (Aldrich) was standardized immediately prior to use using salicylaldehyde phenylhydrazone.[53] The synthesis of butylsodium was as previously published.[54] All synthetic work was carried out under an inert argon atmosphere.

[{Fe(C_5H_3)$_2$}Na$_4$Mg$_4$(*i*-Pr$_2$N)$_8$] (1). In a flame-dried Schlenk tube, 0.8 g (10 mmol) of freshly prepared *n*-butylsodium was suspended in 10 mL of hexane and placed in an ultrasonic bath for 10 minutes. To this suspension, 10 mmol of an *n*,*s*-dibutylmagnesium solution in heptane was then added to yield a brown congealed mass. This was dissolved by the addition of 3 molar equivalents (4.2 mL, 30 mmol) of diisopropylamine. The resultant slightly cloudy solution was heated gently to ensure complete dissolution. Ferrocene (2.5 mmol, 0.48 g) was added to yield an orange solution. This solution was heated to reflux for 15 min, by which time it had turned from orange to red. The majority of the hydrocarbon solvent was removed in vacuo and replaced with 3 mL of toluene. The solution was briefly heated to reflux again to ensure complete dissolution of the red product. A deep red solution was obtained. This solution was slowly cooled by leaving it in a Dewar flask filled with hot water. On reaching ambient temperature, red cubelike crystals of **1** were obtained. Complex **1** is air- and moisture-sensitive and pyrophoric. Yield = 2.11 g, 72%. mp = 161−164 °C. Satisfactory C, H, and N analysis was obtained. From EXSY NMR spectroscopy, it has been shown that two conformations are present in solution in an equal quantity (1:1 ratio of conformer **A** to conformer **B**). ^{1}H NMR (400.13 MHz, benzene-d_6, 300 K): δ 4.22 [4H, d, (C*H*)$_2$, cyclopentadienyl(**A**)], 4.21 [4H, d, (C*H*)$_2$, cyclopentadienyl(**B**)], 3.55 [2H, t, C*H*, cyclopentadienyl(**B**)], 3.52 [16H, m, (CH$_3$)$_2$C*H*, amide(**A** and **B**)], 3.50 [2H, t, C*H*, cyclopentadienyl(**A**)], 3.15 [16H, m, (CH$_3$)$_2$C*H*, amide′(**A** and **B**)], 1.50−1.41 [four overlapping doublets, 96H, (C*H*$_3$)$_2$CH, amide(**A** and **B**)], 1.10−0.95 [four overlapping doublets, 96H, (C*H*$_3$)$_2$CH, amide′(**A** and **B**)]. ^{13}C NMR (100.63 MHz, benzene-d_6, 300 K): δ 87.7 [*C*H, cyclopentadienyl], 86.6 [*C*H, cyclopentadienyl], 86.4 [*C*, cyclopentadienyl], 84.8 [*C*, cyclopentadienyl], 82.4 [*C*H, cyclopentadienyl], 82.1 [*C*H, cyclopentadienyl], 50.1, 49.7, 49.4, 48.4 [four resonances, *C*H, diisopropylamide], and 28.3, 28.1, 28.0, 27.5, 27.0, 26.5, 26.0, and 24.2 [eight resonances, *C*H$_3$, diisopropylamide].

[{Ru(C_5H_3)$_2$}Na$_4$Mg$_4$(*i*-Pr$_2$N)$_8$] (2). In a flame-dried Schlenk tube, 0.32 g (4 mmol) of freshly prepared *n*-butylsodium was suspended in 6 mL of hexane and placed in an ultrasonic bath for 10 minutes. To this suspension, 4 mmol of an *n*,*s*-dibutylmagnesium solution in heptane was then added to yield a brown congealed mass. This was dissolved by the addition of 3 molar equivalents (1.68 mL, 12 mmol) of diisopropylamine. The resultant slightly cloudy solution was heated gently to ensure complete dissolution. Ruthenocene (1 mmol, 0.23 g) was added to yield a yellow solution. This solution was heated to reflux for 15 min, by which time an off-white solid had precipitated. The majority of the hydrocarbon solvent was removed in vacuo and replaced with 2 mL of toluene. The solution was briefly heated to reflux again to ensure complete dissolution of the product. A yellow solution was obtained. This solution was slowly cooled by leaving it in a Dewar flask filled with hot water. On reaching ambient temperature, pale yellow cubelike crystals of **2** were obtained. Complex **2** is air- and moisture-sensitive. Yield = 0.65 g, 53%. mp > 250 °C. Satisfactory C, H, and N analysis was obtained. From EXSY NMR spectroscopy it has been shown that two conformations are present in solution (3:1 concentration ratio of conformer **A** to conformer **B**).^{1}H NMR (400.13 MHz, benzene-d_6, 300 K): δ 4.45 [12H, d, (C*H*)$_2$, cyclopentadienyl-(**A**)], 4.41 [4H, d, (C*H*)$_2$, cyclopentadienyl(**B**)], 3.73 [2H, t, C*H*, cyclopentadienyl(**B**)], 3.68 [6H, t, C*H*, cyclopentadienyl(**B**)], 3.47 [32H (24 from **A** and 8 from **B**), m, (CH$_3$)$_2$C*H*, amide], 3.23 [32H, (24 from **A** and 8 from **B**), m, (CH$_3$)$_2$C*H*, amide], 1.40−1.32 [four overlapping doublets, 196H (144 from **A** and 48 from **B**), (C*H*$_3$)$_2$CH, amide], 1.18−1.06 [four overlapping doublets, 196H (144 from **A** and 48 from **B**), (C*H*$_3$)$_2$CH].^{13}C NMR (100.63 MHz, benzene-d_6, 300 K): δ 86.3 [*C*H, cyclopentadienyl], 84.7 [*C*H, cyclopentadienyl], 82.3 [*C*, cyclopentadienyl], 81.8 [*C*, cyclopentadienyl], 70.4 [*C*H, cyclopentadienyl], 65.9 [*C*H, cyclopentadienyl], 49.1, 48.6, 48.1, 47.9 [four resonances, *C*H,

(52) Abel, E. W.; Coston, T. P. J.; Orrell, K. G.; Sîks, V.; Stephenson, D. *J. Magn. Reson.* **1986**, *70*, 34.
(53) Love, B. E.; Jones, E. G. *J. Org. Chem.* **1999**, *64*, 3755.
(54) Schade, C.; Bauer, W.; Schleyer, P. v. R. *J. Organomet. Chem.* **1985**, *295*, C25.

Table 4. Crystallographic Data for **1**, **2**, and **3**

	1	2	3
empirical formula	$C_{58}H_{118}FeMg_4N_8Na_4$	$C_{58}H_{118}Mg_4N_8Na_4Ru$	$C_{58}H_{118}Mg_4N_8Na_4Os$
formula weight	1172.7	1217.9	1307.0
temp (K)	160	123	123
crystal size (mm^3)	0.70 × 0.60 × 0.50	0.35 × 0.30 × 0.05	0.60 × 0.50 × 0.40
crystal system	monoclinic	monoclinic	monoclinic
space group	$P2_1/n$	$P2_1/n$	$P2_1/n$
a (Å)	16.1070(7)	16.1677(5)	16.1472(2)
b (Å)	15.2446(6)	15.1615(6)	15.1476(2)
c (Å)	16.2557(7)	16.1872(6)	16.1729(2)
β (deg)	118.082(1)	117.288(2)	117.255(1)
volume ($Å^3$)	3521.6(3)	3526.3(2)	3516.57(8)
Z	2	2	2
ρ_{calcd} (g cm^{-3})	1.106	1.147	1.234
μ (mm^{-1})	0.313	0.321	1.912
data measured	29235	15032	85043
unique data, R_{int}	8205, 0.0272	7790, 0.0783	10255, 0.0330
refined parameters	368	368	368
R [$I > 2\sigma(I)$]	0.0357	0.0529	0.0203
R_w (on F^2, all data)	0.1127	0.0942	0.0482
GOF on F^2	1.248	1.019	1.043
max, min el density (e $Å^{-3}$)	0.59, −0.29	0.63, −0.87	0.74, −1.13

diisopropylamide], and 30.2, 27.5, 27.4, 27.3, 26.9, 26.1, 25.7, and 23.7 [eight resonances, *C*H_3, diisopropylamide].

[{Os(C_5H_3)$_2$}Na_4Mg_4(*i*-Pr$_2$N)$_8$] (3). In a flame-dried Schlenk tube, 0.32 g (4 mmol) of freshly prepared *n*-butylsodium was suspended in 6 mL of hexane and placed in an ultrasonic bath for 10 min. To this suspension, 4 mmol of an *n*,*s*-dibutylmagnesium solution in heptane was then added to yield a brown congealed mass. This was dissolved by the addition of 3 molar equivalents (1.68 mL, 12 mmol) of diisopropylamine. The resultant slightly cloudy solution was heated gently to ensure complete dissolution. Osmocene (1 mmol, 0.32 g) was added to yield a pale yellow solution. This solution was heated to reflux for 15 min, by which time a white solid had formed. The majority of the hydrocarbon solvent was removed in vacuo and replaced with 2 mL of toluene. The solution was briefly heated to reflux again to ensure complete dissolution of the product. A pale yellow solution was obtained. This solution was slowly cooled by leaving it in a Dewar flask filled with hot water. On reaching ambient temperature, pale off-white cubelike crystals of **3** were obtained. Complex **3** is air- and moisture-sensitive. Yield = 0.81 g, 62%. mp > 250 °C. Satisfactory C, H, and N analysis was obtained. From EXSY NMR spectroscopy it has been shown that two conformations are present in solution (3:1 concentration ratio of conformer **A** to conformer **B**). ^{1}H NMR (400.13 MHz, benzene-d_6, 300 K): δ 4.56 [12H, d, (C*H*)$_2$, cyclopentadienyl(**A**)], 4.52 [4H, d, (C*H*)$_2$, cyclopentadienyl(**B**)], 3.85 [2H, t, C*H*, cyclopentadienyl(**B**)], 3.77 [6H, t, C*H*, cyclopentadienyl(**A**)], 3.44 [32H (24 from **A** and 8 from **B**), m, (CH$_3$)$_2$C*H*, amide], 3.27 [32H (24 from **A** and 8 from **B**), m, (CH$_3$)$_2$C*H*, amide], 1.36−1.29 [four overlapping doublets, 196H (144 from **A** and 48 from **B**), (CH$_3$)$_2$CH, amide], 1.19−1.09 [four overlapping doublets, 196H (144 from **A** and 48 from **B**), (C*H*$_3$)$_2$CH, amide]. ^{13}C NMR (100.63 MHz, benzene-d_6, 300 K): δ 79.1 [*C*H, cyclopentadienyl], 77.1 [*C*H, cyclopentadienyl], 75.9 [*C*, cyclopentadienyl], 75.7 [*C*, cyclopentadienyl], 74.8 [*C*H, cyclopentadienyl], 65.8 [*C*H, cyclopentadienyl], 49.1, 48.6, 48.1, 47.9 [four resonances, *C*H, diisopropylamide], and 30.1, 27.6, 27.5, 27.4, 26.9, 26.0, 25.7, and 23.7 [eight resonances, *C*H_3, diisopropylamide].

***n*,s-Bu$_2$Mg NMR Analysis.** A volume of 0.5 mL of a 1 M commercial solution of DBM in heptane was placed in a Schlenk tube, and the solvent was removed under vacuum. The solid residue was then dissolved in deuterated benzene (0.6 mL). ^{1}H and ^{13}C NMR spectra were recorded. ^{1}H NMR (400.13 MHz, 293K, benzene-d_6): δ 3.73 (m, OC*H*$_2$, OC*H*), 3.42 1.68−0.68 (m, broad, CH$_2$'s, CH$_3$'s aliphatics), 0.54−(−0.3) (m, broad, Mg−C*H*2), −0.68 (m, broad, Mg−C*H*). ^{13}C{H} NMR (100.63 MHz, 293K, benzene-d_6): δ 64.6 (OCH$_2$, OCH), 38.0, 37.6, 31.2, 29.4, 29.1, 20.2, 19.6, 14.2, 14.1, 13.9, (*C*H$_2$'s, *C*H$_3$'s aliphatics), 9.4, 9.6 (Mg-*C*H$_2$, Mg-*C*H). ^{1}H NMR (400.13 MHz, 360K, benzene-d_6): δ 3.73 (m, OC*H*$_2$, OC*H*), 3.42 [quartet (7.05 Hz), OC*H*$_2$, OC*H*], 1.68 [quintet (7.89 Hz), CH$_2$'s aliphatics], 1.49 [sextet (7.2 Hz) CH$_2$'s aliphatics], 1.35 (m, CH$_2$'s aliphatics), 0.99 [t (7.2 Hz), CH$_3$'s aliphatics], 0.35−0.12 (m, broad, Mg−C*H*), −0.64 (m, broad, Mg−C*H*$_2$).

X-ray Crystallography. Crystal data and other information on the structure refinements are given in Table 4. Data were collected on Bruker SMART (**1**) and Nonius KappaCCD (**2** and **3**) diffractometers with Mo Kα radiation (λ = 0.71073 Å), using standard procedures and software.[55] Absorption corrections were semiempirical, based on symmetry-equivalent and repeated measurements.[56] The structure of **1** was solved by direct methods,[57] and the others are isostructural; the same atom numbering was used for all structures for ease of comparison. Refinement was on F^2 values for all unique data in each case.[57] H atoms were constrained with a riding model, except for those of the Cp rings, which were located in difference maps and refined freely with individual isotropic displacement parameters. In all three structures, the transition metal atom lies on a crystallographic inversion center.

Acknowledgment. We gratefully acknowledge the continued financial support of the U.K. EPSRC through Grant Award No. GR/R81183/01.

Supporting Information Available: X-ray crystallographic data for **1**, **2**, and **3** (CIF). This material is available free of charge via the Internet at http://pubs.acs.org.

JA0472230

(55) (a) *SMART* and *SAINT* software; Bruker AXS: Madison, WI, 1994−2001. (b) *COLLECT* software; Nonius BV: Delft, The Netherlands, 1998. (c) Otwinowski, Z.; Minor, W. In *Macromolecular Crystallography*; Carter, C. W., Jr., Sweet, R. M., Eds.; Methods in Enzymology; Academic Press: New York, 1997; Vol. 276, Part A, pp 307−326.
(56) (a) Blessing, R. H. *Acta Crystallogr., Sect. A* **1995**, *51*, 33. (b) Sheldrick, G. M. *SADABS*; University of Göttingen: Göttingen, Germany, 2001.
(57) (a) Sheldrick, G. M. *SHELXL97*; University of Göttingen: Göttingen, Germany, 2001. (b) Sheldrick, G. M. *SHELXTL* version 6; Bruker AXS: Madison, WI, 2001.